Accepted Manuscript

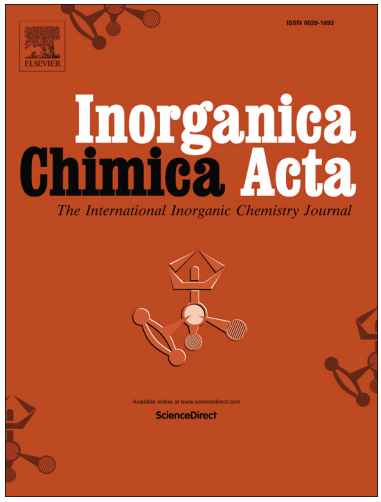

A comparative analyses of bioactive Cu(II) complexes using Hirshfeld surface and Density Functional Theory (DFT) methods: DNA binding studies, Cleavage and Antibiofilm activities

Mohammad Usman, Farukh Arjmand, Musheer Ahmad, Mohammad Shavez Khan, Iqbal Ahmad, Sartaj Tabassum

PII: S0020-1693(16)30463-7
DOI: http://dx.doi.org/10.1016/j.ica.2016.08.011
Reference: ICA 17205

To appear in: *Inorganica Chimica Acta*

Received Date: 8 June 2016
Revised Date: 5 August 2016
Accepted Date: 6 August 2016

Please cite this article as: M. Usman, F. Arjmand, M. Ahmad, M.S. Khan, I. Ahmad, S. Tabassum, A comparative analyses of bioactive Cu(II) complexes using Hirshfeld surface and Density Functional Theory (DFT) methods: DNA binding studies, Cleavage and Antibiofilm activities, *Inorganica Chimica Acta* (2016), doi: http://dx.doi.org/10.1016/j.ica.2016.08.011

A comparative analyses of bioactive Cu(II) complexes using Hirshfeld surface and Density Functional Theory (DFT) methods: DNA binding studies, Cleavage and Antibiofilm activities

Mohammad Usman[a], Farukh Arjmand[a], Musheer Ahmad[b], Mohammad Shavez Khan[c], Iqbal Ahmad[c] and Sartaj Tabassum[a*]

[a]*Department of Chemistry, Aligarh Muslim University, Aligarh, 202002, India.*
[b]*Department of Applied Chemistry, ZHCET, Aligarh Muslim University, Aligarh, 202002, India.*
[c]*Department of Agricultural Microbiology, Aligarh Muslim University, Aligarh, 202002, India.*
E–mail address: tsartaj62@yahoo.com +91 9358255791, [*]*Corresponding author: Aligarh Muslim University, Aligarh, UP–202002, India.*

Keywords: Single crystal X-ray structure; DFT; Hirshfeld surface analyses; *In vitro* DNA binding; pBR322 DNA cleavage; Antibiofilm activity.

Abbreviations

dip	[{(2,6-diisopropylphenyl)imino}methyl]phenol
dimp	[{(2,6-diisopropylphenyl)imino}methyl]-6-methoxyphenol
CT DNA	Calf thymus DNA
EB	Ethidium bromide
QM	Quantum mechanical

Abstract

Two mononuclear Copper(II) complexes, $[Cu(dip)_2]$ (**1**) and $[Cu(dimp)_2]$ (**2**) have been synthesized and characterized thoroughly by various spectroscopic techniques and single crystal X-ray diffraction analysis. Dispersion corrected B3LYP/DFT calculations have been carried out to elucidate the tentative assignments of N-Cu-N/O-Cu-O/O-Cu-N and other significant vibrational modes. Additionally, quantitative analysis of intra and intermolecular non-covalent interactions were carried out using Hirshfeld surface calculations to explore H-bonding, C-H/π and Cu…H-C interactions. *In vitro* DNA binding studies of **1** and **2** were performed by employing optical spectroscopic techniques. The cleavage activity of **1** and **2** with pBR322 plasmid DNA was carried out by gel electrophoretic assay and it was observed that both **1** and **2**

cleaved DNA by oxidative pathway via ROS species *viz*., $O_2^{\bullet-}$, $^1O_2$ etc. Furthermore, antibiofilm activity of the complexes **1** and **2** was evaluated against *E. Coli* 25922 and it was found to interfere and inhibit the biofilm forming ability of *E. Coli* 25922.

1. Introduction

Biofilm formation by pathogenic bacteria is considered a major step for establishing successful colonization on implanted medical devices, stents, catheter and endocarditis or lung infections in hospitals [1]. These biofilms being tolerant to both antibiotics and immune system are therefore difficult to treat and result in severe pathological conditions for host [2]. There is therefore, a huge demand of efficacious therapeutic molecules for combating bacterial biofilms, and new innovative strategies are required for the development of novel, potent as well as less toxic antibacterial agents [3].

In recent past, much attention has been focused for the development of DNA targeted antimicrobials [4] as previous literature reveals that DNA is an important primary cellular target for most of the therapeutic drugs in clinical use [5]. Considering the role of DNA (both extracellular and intracellular) in the development and maturation of biofilms [6], DNA targeting molecules can be considered as potential antibiofilm agents. Therapeutic agents exert their cytotoxic and antibacterial effect by binding to DNA, thereby cleaving the DNA and inhibiting the growth of the cells, preventing further aggregation or uncontrolled division of cells leading to colonization [7].

Currently, tremendous efforts are directed for the design and synthesis of metal-based therapeutics and much focus is on the development of DNA- targeted drug candidates involving the interactions with specific domain of DNA helix preferably by non-covalent mode (*viz.,* intercalation, groove binding and surface interaction with negatively charged oxygen atoms of

the phosphate linkage) [8]. Among the metal ions utilized in drug design, copper being an endogenous bio-essential element plays a pivotal role in the functioning of several metalloenzymes and proteins [9]. Due to its high redox activity, copper has potential to catalyze the generation of reactive oxygen species (ROS), interrupt the redox equilibrium of cell and also intervene in the redox mediated cellular signaling pathways [10]. It is speculated that ROS are capable of inducing DNA strand scission and altering various cellular component like proteins, lipids and nucleic acids resulting in oxidative or hydrolytic damage of cells [11]. Moreover, the design of ligand framework has a significant impact on tuning and modulating the specificity of tailored drug candidate towards the biological target. Therefore, the coordination between copper ion and pharmacophore scaffold provides a high potency, specificity and efficacy to the drug entity for their biological target [12]. Among the several organic ligands, our interest stems in Schiff bases derived from o-vanillin and salicylaldehyde, as their metal complexes are known to exhibit diverse biological applications *viz*., antitumor, anti-inflammatory, antiviral, antibacterial and cell imaging agents [13].

Molecular self-assembly through weak non-covalent forces is the hallmark of biological systems. Amongst a number of non-covalent forces *viz.,* H-bonding, C···H, C-H/π, π···π, cation/anion···π, lone-pair···π, metal···H interactions etc. have been utilized in directing molecular assembly for the synchronization of several biochemical processes [14]. These non-covalent interactions have been demonstrated to play a key role in physicochemical properties, molecular recognition, drug receptor interaction, antigen-antibody recognition, enzymatic inhibition and protein folding [15].

Herein, we present the fully characterized Cu(II) complexes **1** and **2,** derived from Schiff base ligands 2-(((2,6-diisopropylphenyl)imino)methyl)-6-methylphenol, dip, and 2-[((2,6-diisopropylphenyl)imino)methyl)-6-methoxyphenol, dimp, structure elucidation of complexes

was done by single crystal X-ray diffraction analysis. Density Functional Theory (DFT) methods were employed to calculate electronic structure, HOMO-LUMO gap, atomic charges and vibrational frequencies of metal-ligand linkages. The antibiofilm activity against *E. Coli* 25922, DNA binding profile and DNA cleavage experiment with pBR322 DNA was carried out for both the complexes **1** and **2**.

2. Experimental

2.1. Materials

All reagents were commercially available and used as supplied without further purification. Copper nitrate trihydrate (Merck), o-vanillin (Sigma-Aldrich), 2, 6-Diisopropyl-aniline (Merck) and Calf thymus DNA (CT DNA) (Sigma–Aldrich), supercoiled plasmid DNA pBR322 (Genei) were utilized as received.

2.2. Methods and instrumentation

Microanalyses for the copper complexes were performed using a CE–440 elemental analyzer (Exeter Analytical Inc.). Infrared spectra were obtained (KBr disk, 400–4000 cm^{-1}) on a Perkin–Elmer Model 1320 spectrometer. EPR spectra of copper complexes was recorded at X-band (9.167 GHz) at room temperature on JEOL FA-200 continuous-wave spectrophotometer using Mn as standard (g=2.0036). Electronic spectra was recorded on PerkinElmer UV–vis spectrophotometer. Fluorescence measurements were carried out on a RF–5301 PC spectrofluorophotometer (Schimadzu). DNA cleavage experiments were performed with the help of Axygen made electrophoresis supported by a Genie power supply with a potential range of 50–500 volts, visualized and photographed by a Vilber–INFINITY gel documentation system.

*2.3. Synthesis of [Cu(dip)$_2$] (**1**)*

A methanolic solution of salicylaldehyde (10 ml, 4 mmol) was mixed with methanolic solution of 2,6-diisopropylaniline (5 ml, 4 mmol). The mixture was stirred for 2h at 70 ^{0}C to give a clear deep yellow solution. To the above reaction mixture, methanolic solution of $Cu(NO_3)_2.3H_2O$ (5 ml) was added which was refluxed for 4 h, until dark brown solution resulted. The completion of reaction was monitored by TLC. After completion of the reaction, the mixture was reduced in volume by heating on hot plate and filtered under hot condition. On slow evaporation of filtrate, deep brown colored crystals were obtained after 6-7 days. The crystals obtained washed with acetone and air dried. Yield 78%, M.P 180 ^{0}C. Anal. Calc. for [$C_{40}H_{48}CuN_2O_4$] (%): C, 70.20; H, 7.02; N, 4.09; Found: C, 70.26; H, 7.09; N, 4.04. FT-IR (KBr pellet) 1605 cm^{-1} (s, C=N); 2870 cm^{-1} (s, CH_3); 3057 cm^{-1} (s, Ar-CH). UV-vis (1×10^{-4} M, MeOH, λ_{max} nm): 242, 272, 368, 590 nm. Molar conductance: Λ_M (1×10^{-3} M, DMSO): 1.53 Ω^{-1} cm^2 mol^{-1} (non-electrolyte).

*2.4. Synthesis of [Cu(dimp)$_2$] (**2**)*

Yield 82%, M.P 163 ^{0}C. Anal. Calc. for [$C_{38}H_{44}CuN_2O_2$] (%): C, 73.11; H, 7.10; N, 4.49; Found: C, 73.19; H, 7.21; N, 4.61. FT-IR (KBr pellet) 1608 cm^{-1} (s, C=N); 2869 cm^{-1} (s, CH_3); 3061 cm^{-1} (s, Ar-CH). UV-vis (1×10^{-4} M, MeOH, λ_{max} nm): 238, 284, 378, 595 nm. Molar conductance: Λ_M (1×10^{-3} M, DMSO): 1.42 Ω^{-1} cm^2 mol^{-1} (non-electrolyte).

2.5. Description of X–ray Crystal structure

Single crystal X–ray data of complex **1** and **2** was collected at 100 K on a Bruker SMART APEX CCD diffractometer using graphite monochromatic MoK_α radiation (λ = 0.71073 Å). The linear absorption coefficients, scattering factors for the atoms and the anomalous dispersion corrections were referred from the International Tables for X–ray Crystallography. The data integration and reduction were worked out with SAINT software. Empirical absorption correction was applied to

the collected reflections with SADABS program [16] and the space group was determined using XPREP. The structure was solved by direct methods using SHELXTL–97 and refined on F^2 by full–matrix least–squares using the SHELXTL–97 programme package [17]. Only a few H atoms could be located in the difference Fourier maps in the structure. The rest were placed at calculated positions using idealized geometries (riding model) and assigned fixed isotropic displacement parameters. All non–H atoms were refined anisotropically. Several DFIX commands were used for fixing some bond distances in complex **1** and **2**. The crystal and refinement data are collected in Table 1. Selective bond distances and angles are given in Table S1 and S2.

Table 1. Crystal and Structure Refinement Data for complexes **1** and **2**.

Parameters	**1**	**2**
CCDC No.	971306	1006580
Formula	$C_{38}H_{44}CuN_2O_2$	$C_{40}H_{48}CuN_2O_4$
Fw (g mol^{-1})	624.30	684.34
Crystal System	Triclinic	Triclinic
Space Group	*P*–1	*P*–1
a (Å)	7.910(5)	10.899(5)
b (Å)	10.199(5)	15.981(5)
c (Å)	11.138(5)	22.961(5)
α (deg)	113.824(5)	97.395(5)
β (deg)	97.275(5)	103.101(5)
γ (deg)	97.646(5)	108.274(5)
U ($Å^3$)	798.4(7)	3611(2)
Z	1	4
ρ_{calc} (g/cm^3)	1.298	1.259
μ (mm^{-1})	0.720	0.647
F(000)	331	1452
Crystal size (mm)	0.26 × 0.19 × 0.16	0.25 × 0.18 × 0.15
Temp (K)	100	100
Measured reflns	4256	18205
Unique reflns	2577	8646
θ Range (deg)/completeness (%)	2.04 to 25.50/0.972	0.93 to 25.00/ 0.977
GOF[a]	1.154	1.132
Final R[b] indices	R_1 = 0.0529	R_1 = 0.0805

$[I>2\sigma(I)]$	wR_2 = 0.1335	wR_2 = 0.2626
R^b indices (all data)	R_1 = 0.0678 wR_2 = 0.1907	R_1 = 0.1220 wR_2 = 0.3013

[a]GoF is defined as $\{\Sigma[w(F_0^2-F_c^2)]/(n-P)\}^{1/2}$ where n is the number of data and p is the number of parameters. [b]$R = \{\Sigma||F_0|-|F_c||/\Sigma|F_0|$, $wR^2 = \{\Sigma\, w(F_0^2-F_c^2)^2 / \Sigma\, w(F_0^2)^2\}^{1/2}$.

2.6. Theoretical Calculations

The density functional theory (DFT) calculations were done with the ORCA 3.0.1 computational package [18]. The geometry optimization was carried out by hybrid B3LYP functional [19] using the Aldrich's def2–TZVP basis set for copper atom and def2–SVP basis set for C, H, O, N atoms [20]. The optimized structure was further re-calculated using def2–TZVP basis set for all atoms to calculate the HOMO and LUMO energies. The initial geometry was taken from the single-crystal X-ray data and subjected to optimization. To accelerate the calculations we utilized the resolution of identity (RI) approximation with the decontracted auxiliary def2-SVP/J and def2–TZV/J Coulomb fitting basis sets and the chain–of–spheres (RIJCOSX) approximation to exact exchange as implemented in ORCA [21]. Furthermore, analytical vibrational frequency calculations were performed on the optimized geometries of complexes **1** and **2** using same basis set parameters. The scaling factor 0.9572 for Cu(II) complexes have been applied on the wavenumber regions from 500-4000 cm^{-1} for a better correlation with experimental spectra.

Hirshfeld surface were mapped using Crystal Explorer [22] software using crystal structure coordinates of CIF files.

The molecular docking studies have been performed by using AutodockVina version 1.1.2 [23]. All rotatable bonds within the ligand were allowed to rotate freely and receptor was considered rigid. The crystal structure of the B–DNA dodecamer $d(CGCGAATTCGCG)_2$ (PDB ID: 1BNA)

was retrieved from the protein data bank (http://www.rcsb.org./pdb). Visualization of minimum energy favorable docked poses has been performed using Discovery studio 4.1 and PyMol [24].

2.7. DNA Binding and cleavage Experiments

DNA binding experiments include absorption spectral traces, emission spectroscopy and circular dichroism conformed to the standard methods and practices previously adopted by our laboratory [25] whereas DNA cleavage was performed by the standard protocol as described previously [26]. While measuring the absorption spectra an equal amount of DNA was added to both the compound solutions and the reference solution to eliminate the absorbance of the CT–DNA itself, and Tris–HCl buffer was subtracted through base line correction. All the experiments involving interaction of the complexes with CT–DNA were performed in double distilled buffer containing tris(hydroxymethyl)aminomethane and adjusted to pH 7.3 with hydrochloric acid. Solution of CT–DNA in buffer gave a ratio of UV absorbance at 260 and 280 nm of *ca*. 1.9:1 indicating that DNA was sufficiently free of protein. The DNA concentration per nucleotide was determined by absorption spectroscopy with the molar absorption coefficient 6600 $M^{-1}cm^{-1}$ at 260 nm.

2.8. Biofilm inhibition Assay

Minimum inhibitory concentration (MIC) of compound was determined against standard strain of *E. Coli* and Sub-MICs were selected for the assessment of anti-biofilm activity. Antibiofilm potential of Sub MICs of the complex **1** was measured using the polyvinyl chloride biofilm formation assay [27] Briefly, overnight (treated and untreated) culture of *E. coli 25922* were visualized for biofilm formation by staining with 0.1% crystal violet solution. The 96-well microtiter plates were rinsed to remove planktonic cells, and the surface-attached cells were then quantified by solubilizing the dye in ethanol and measuring the absorbance at OD_{470}. Further

biofilm formed on glass coverslip were visualized under light microscope and under scanning electron microscope using briefly modified method as described earlier [28].

3. Result and discussion

The *in situ* condensation reaction of the o-vanillin/salicylaldehyde and 2,6-diisopropylaniline in 1:1 molar ratio resulted in the deep yellow colored ligand (dip and dimp) and subsequently its mononuclear copper complexes **1** and **2** were synthesized with $Cu(NO_3)_2.3H_2O$. Both the complexes were characterized by elemental analysis, UV-vis, EPR and FTIR and single crystal X-ray studies. Complexes are air-stable and miscible in MeOH, DMF, MeCN and DMSO. Complexes **1** and **2** were predesigned to validate their recognition with specific domain of DNA helix and for bacterial bioflim inhibition activity.

3.1. Structure description

Crystal structures of complexes **1** and **2** were solved by single crystal X-ray diffraction analysis at 100 K. Note that the crystal framework of **1** and **2** have been already reported in the literature [29] but the Space group and crystal lattice parameters of our crystal systems are totally different due to some experimental conditions specially temperature and measured parameters.

Single crystal X-ray study showed that the complex **1** crystallized in the triclinic crystal system. Fig. 1a depicts the ORTEP structure of complex **1** and Tables S1 show the selected bond lengths and angles. The structure was successfully solved and converged in the space group *P*–1. The asymmetric unit consists of half Cu(II) ion (sit on the special position having two-fold axis of symmetry) and one Schiff base ligands dip. The complex **1** showed square planar CuO_2N_2 coordination geometry with ligation from two nitrogen atoms (Cu–N = 2.015(3) Å) and two oxygen atoms (Cu–O = 1.876(3) Å) from ligands dip. All the Cu–O and Cu–N bond distances

are within the range reported for square planar Cu(II) complexes [30]. 2D supramolecular architecture is depicted in Fig. S1.

Complex **2** also crystallized in the triclinic crystal system with space group *P*–1. However, the asymmetric unit consists of two molecules and each molecule contains one Cu(II) ion and two Schiff base ligands dimp. Fig. 1b depicts the ORTEP structure of complex **1** and Tables S2 show the selected bond lengths and angles. The complex **2** exhibited distorted square planar CuO_2N_2 coordination geometry with ligation from two nitrogen atoms (Cu–N = 1.970(6) – 1.991(5) Å) and two oxygen atoms (Cu–O = 1.875(4) – 1.875(4) Å) from two different ligands moieties. All the Cu–O and Cu–N bond distances are within the range reported for distorted square planar Cu(II) complexes [31]. Contrary to **1**, it shows some deviation from orthogonality which could be attributed to the presence of steric crowding at both phenyl rings of the Schiff base ligand. The steric hindrance caused by isopropyl groups is many folds stronger than that caused by methoxy moieties, therefore the orthogonality could not be achieved. 2D supramolecular structure (Fig. S2) was generated which was stabilized by multipoint weak H–bonding and strong -CH‑π aromatic stacking arrangement between two neighboring phenyl moieties as depicted in Fig. S3.

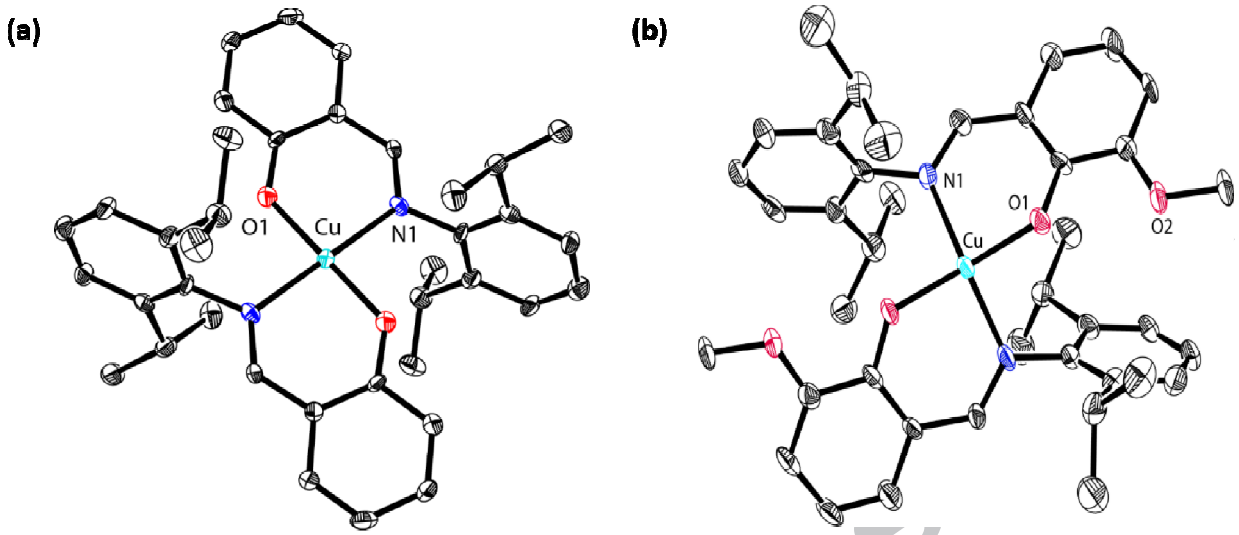

Fig. 1. X–ray molecular structure of the (a) complex **1** and (b) complex **2**, along with labeling of atoms. Thermal ellipsoids were shown at 50% probability. Hydrogen atoms have been omitted for clarity.

3.2. Spectral characterization

The structure of complexes **1** and **2** was also validated by other spectroscopic techniques viz EPR, UV-vis and FT-IR spectroscopy.

EPR studies of polycrystalline samples of complexes **1** and **2** recorded at room temperature (Fig. S4) exhibited $g_{\parallel}$ and $g_{\perp}$ values of 2.12-2.09 and 2.06-2.06, respectivily, while g_{av} values was determined to be 2.08-2.07 from the relation $g_{av}^2 = 1/3(g_{\parallel}^2+2g_{\perp}^2)$. These calculated data are in agreement with an orbitally non-degenerate state for four-coordinate Cu(II) complexes . The value of $g_{\parallel} > g_{\perp} > 2.0023$ revealed that the unpaired electron was most likely to be localized in the $d_{x^2-y^2}$ ground state, and a square based geometry proposed for the complexes [32]. The experimental $g_{\parallel}$ values for complexes were less than 2.3, in agreement with the covalent character of the M-L bond [33].

The ESI mass spectrum of complexes **1** revealed a characteristic molecular ion peak at *m/z* 624.8 attributed to the $[C_{35}H_{44}CuN_2O_2 + H^+]$ moiety. Fragmentation peaks at m/z 279.2, 180.9 were

observed for [$C_{19}H_{22}NO + 2H^+$] and [$C_7H_5CuNO + H^+$], respectively (Fig. S5). For complex **2**, molecular ion peak at m/z 685.2 attributed to [$C_{40}H_{48}CuN_2O_4 + H^+$] moiety and fragmentation peak at m/z 312.1 observed for [$C_{20}H_{24}NO_2 + 2H^+$] species (Fig. S6).

The electronic spectra of complex **1** was recorded in MeOH revealed two well resolved absorption peaks at 242 and 272 nm corresponding to π–π* intraligand transition; a broad absorption maxima at 368 nm was attributed to LMCT transition (Fig. S7). A very weak and broad d-d transition envelop observed at 590 nm in the visible region was consistent with square planar environment around the Cu(II) center [34]. In complex **2,** bands were observed at 238, 284 nm (π–π*) and broad band around 378 nm (LMCT). A low intensity shoulder band was also observed at 595 nm adjacent to d-d band, consistent with the distorted square planar geometry of Cu(II) ion.

3.3. Density functional theory

The gas phase structure optimization of copper complexes are performed at B3LYP/DFT level and calculated bond lengths, angles and Mulliken charges are given in Table S1, S2 and S3. The calculated bond lengths are longer than the experimental data because the former were optimized in the gas phase and latter were in tight crystal lattice.

3.3.2. FT-IR spectroscopy vs. vibrational mode analyses

The proper assignment of metal framework vibrations in far-IR region was challenging due to the higher mixture of the different internal coordinates that take part in the normal modes. Therefore, DFT calculations were undertaken to provide better insight in the involvement of vibrational dynamics of metal-based drug entities. The calculations predict all 3N-6 vibrational mods with real frequencies, which ranges from 35 cm^{-1} to about 3212 cm^{-1}. DFT results revealed the several types of metallic core dynamics (a) Out-of-plane vibrations and (b) In-plane

vibrations. Various type of out-of-plane vibrations predicted below 350 cm^{-1} and In-plane vibrations predicted above 350 cm^{-1}. The experimental and simulated spectra of complexes **1** and **2** are shown in Fig.S8-S15. Slight variation have been observed in simulated spectra because experimental values contained both harmonic and anharmonic vibrational frequencies while calculated one depicts only harmonic vibrations. The observed as well as theoretical vibrational modes correspond to in plane bending, out of plane rocking, stretching and in-plane rocking are depicted in Table 2 and S4. Some **animated images** of significant modes of vibration with displacement vectors have also been included in supplementary material.

Table 2. Selected experimental Far-IR and DFT calculated spectra for complexes **1**-**2**, (wavenumber in cm^{-1}).

Complex **1**		Complex **2**		Assignment
Experimental	DFT	Experimental	DFT	
53.27	60.43	60.17	61.13	$_{\Upsilon}$N-Cu-N
102.19	113.42	103.77	119.50	$_{\Upsilon}$O-Cu-O
142.33	149.35	156.37	157.12	$_{\Upsilon}$O-Cu-O
203.02	204.11	205.82	205.81	$_{\Upsilon}$O-Cu-O
219.02	218.06	229.69	230.22	$_{\Upsilon}$N-Cu-N
259.18	263.27	251.38	266.82	$_{\Upsilon}$O-Cu-O, $_{\Upsilon}$N-Cu-N, $_{\tau}CH_3$
290.09	292.07	291.11	292.89	$_{\nu}$O-Cu-O, $_{\delta}$N-Cu-N
328.82	330.45	324.08	325.62	$_{\pi}$O-Cu-N
345.31	350.74	340.27	345.58	$_{\Upsilon}$N-Cu-N, $_{\Upsilon}$N=CH
		369.21	372.12	$_{\Upsilon}$O-C(ϕ)- C(ϕ)-O,
402.19	405.02	405.29	407.21	$_{\delta}$O-Cu-O, $_{\delta}$N-Cu-N
433.42	437.37	440.12	445.42	$_{\delta}$O-Cu-N
464.27	470.81	472.25	477.03	$_{\pi}$O-Cu-O, $_{\pi}$N-Cu-N
524.07	533.87	524.67	538.6	$_{\rho}$O-Cu-N
589.24	595.12	582.04	590.18	$_{av}$O-Cu-O
617.08	620.98	618.12	626.12	$_{sv}$N-Cu-N, $_{sv}$O-Cu-O

sv, symmetrical stretching; av, anti-symmetrical stretching; δ, in-plane bending; ϒ, out-of-plane bending; ρ, in-plane rocking; π, out-of-plane rocking.

3.3.3. Frontier molecular orbital analysis

Frontier molecular orbitals (HOMO and LUMO) play an important role to exemplify the chemical reactivity, kinetic stability and electrical transport properties of the molecule. Recently, the HOMO-LUMO energy gap has been used to verify the bioactivity from intramolecular charge transfer (ICT) and was also correlated with various biological activities like antibacterial, antioxidant and DNA binding studies [35]. A small gap of HOMO-LUMO of molecule was associated with a noteworthy degree of intramolecular charge transfer (ICT) from the electron-donor groups to the electron-acceptor groups through a π-conjugated path. A large HOMO-LUMO gap implies high stability of the molecule in the sense of its lower reactivity in chemical and biochemical reactions [36]. Systems having high E_{HOMO} are good electron donors while those having low E_{LUMO} are good electron acceptors. The calculated energy gap between HOMO and LUMO of complexes **1** and **2** were found to be -3.84 and -3.61 eV (Fig. 2). Previous literature reports have proven the fact that higher HOMO energy of DNA and lower LUMO energy of the interacting molecule reflect much stronger binding propensity, because "electronic charge density" facilitates more easily from the HOMO of the DNA molecule to the LUMO of the interacting molecule and consequently, a stronger interaction between DNA and the interacting molecules takes place.

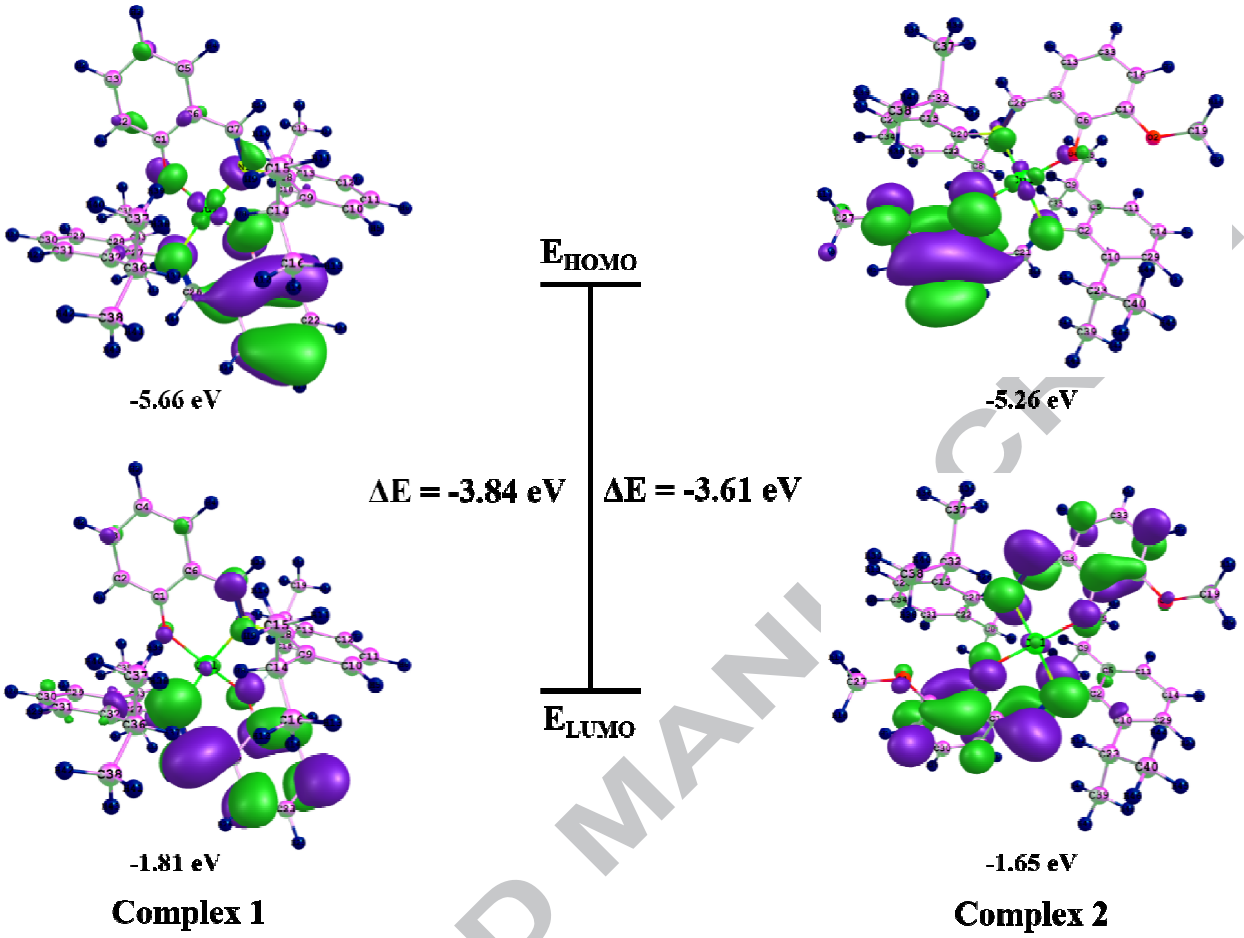

Fig. 2. Diagrammatic representation of Frontier Molecular Orbitals for complex **1** and **2.**

3.4. Hirshfeld surface analyses

The Hirshfeld surfaces of complexes **1** and **2** are illustrated in Fig. S16, depicting surfaces that have been mapped over a d_{norm} range of -0.5 to 1.5 Å, shape index (-1.0 to 1.0 Å) and curvedness (-4.0 to 0.4 Å). The parameter d_{norm} displayed a surface with a red-white-blue color scheme, whereas deep red spots highlighted show shorter contacts *viz*., hydrogen bonding. The white areas represent contacts around the van der Waals separation like H···H contacts and the blue regions are devoid of such close contacts. On the Hirshfeld surface mapped with shape index function, one can examine both red regions corresponding to C-H···π interactions as well as 'bow-tie patterns' which indicated the presence of aromatic stacking (π···π) interactions. The

curvedness surface indicated the electron density of surface curves around the molecular interactions. The fingerprint plots of complexes **1** and **2** are presented in Fig. S17 and S18, can be disintegrated to highlight particular atom-pair close contacts. This itemization allows parting of contributions from different interaction types, which overlap in the full fingerprint. For complex **1**, the proportions of H···H, C···H and C···C interactions comprises 80%, 18.1% and 1.9% of the total Hirshfeld surface for each molecule, respectively. In the case of complex **2**, the proportions of H···H, O···H, C···H, O···C and C-H···Cu (anagostic) interactions encompasses 78.5%, 5.4%, 14.8%, 0.6% and 0.5% of the total Hirshfeld surface for each molecule, respectively [37].

3.5. DNA Binding studies

The binding propensity of complex **1** and **2** with CT–DNA was studied using electronic absorption spectroscopy. Upon successive additions of CT-DNA ($0.0\text{-}2.0\times10^{-4}$ M) to a fixed concentration of complexes **1** and **2** (6.67×10^{-5} M), a concomitant increase in the absorption intensity at the interaligand absorption bands (272 nm for **1** and 284 nm for **2**) with a blue shift of 2-6 nm and a decrease in intensity at the LMCT band (368 for **1** and 378 nm for **2**) with no shift was observed (Fig. 3).

The observed strong hyperchromic shift (53% and 64% in complexes **1** and **2**, respectively) and weak hypochromic shift (12% and 32% in complexes **1** and **2**, respectively) could be attributed to electrostatic mode of interaction of complexes **1** and **2** with partial intercalation [38]. The observed hyperchromism is due to external contact with DNA while hypochromism could be attributed to the base pair stacking interaction between the aromatic chromophore ligand moiety of the complexes **1** and **2** and CT-DNA while the substituted isopropyl groups on position-2, 6 of the Schiff base ligand could favor the hydrophobic contacts within the interior of DNA helical

sites. Further, quantification of the binding strength of complexes **1** and **2** towards the CT-DNA were ascertained by the intrinsic binding constant, K_b values calculated using the Wolfe-Shimer equation [39]. K_b values for complexes **1** and **2** were found to be 2.15(±0.09) × 10^4 and 5.63(±0.12) × 10^4 M^{-1}, respectively. For explaining the greater binding affinity of the complex **2** we utilizes the results of frontier molecular orbital and Hirshfeld surface analysis. As we know that lower LUMO energy of the complex, greater will be the binding affinity and complex **2** has lower LUMO energy (3.61 eV) as compare to complex **1** (3.84 eV). Additionally, molecular docking studies also confirmed the greater binding affinity of complex **2** (section 3.8).

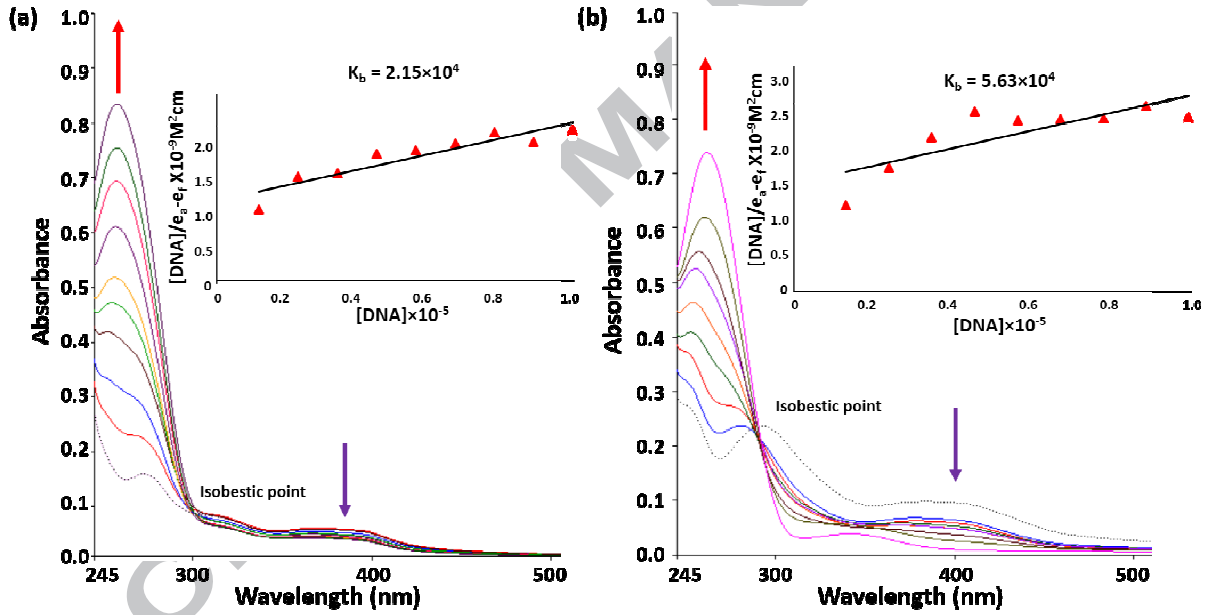

Fig. 3. UV–vis spectra of (a) complex **1** and (b) complex **2**,in Tris–HCl buffer at pH 7.2 upon addition CT–DNA, [DNA] = 0.00–1.8 x 10^{-4} M, [Complexes **1-2**] = 1.0 x 10^{-4} M. Arrow indicates change in absorbance with increasing concentration of CT–DNA.

Fluorescence studies were carried out to get further insights into the binding event of complexes **1** and **2**. No luminescence was observed for the complexes **1** and **2** at room temperature in

aqueous solution, in any organic solvent, or in the presence of CT-DNA. So, the binding of complexes **1** and **2** with DNA cannot be directly predicted through the emission spectra. Therefore, interaction of complex **1** and **2** with DNA were evaluated by a competitive binding experiment using ethidium bromide (EB) as a probe. EB is a phenanthridine fluorescence dye, which emits intense fluorescence in the presence of DNA at 595 nm (λ_{em}) due to its strong intercalation between the adjacent base pairs [40]. In our experiments, it was observed that upon successive addition of **1** and **2** to EB bound DNA system, emission intensity decreased progressively (Fig. S19), indicative of competition between EB and complexes **1** and **2** towards CT-DNA binding.

A decrease in the emission intensities was attributed to the displacement of EB from EB-DNA system, leading to the energy/electron transfer from the guanine base of DNA to MLCT of the complexes **1** and **2**, suggesting their strong competition for the intercalative binding site [41]. Since EB was not completely displaced, partial intercalation in addition to the electrostatic mode of interaction cannot be ruled out. Furthermore, Fluorescence quenching extent was determined qualitatively by using the Stern-Volmer equation [42]. The K_{SV} value for complexes **1** and **2** were found to be $4.93(\pm0.07) \times 10^4$ M^{-1} and $5.03(\pm0.11) \times 10^4$ M^{-1}, respectively.

The precondition of good DNA binding agents was fulfilled by drug entities **1** and **2** as confirmed by UV-vis titration and florescence quenching experiments, another quite sensitive optical spectroscopy *viz.*, circular dichroic technique was carried out to capture the conformational changes during drug – DNA interactions. The CD spectra of CT DNA consists of a positive band at 280 nm due to base-pair π - π stacking and a negative band at 245 nm due to right handed helicity which is characteristic of DNA in the right B-form [43]. An intercalative mode of interaction enhances the intensity of both bands while no or less perturbation is

attributed for groove and electrostatic binding. Upon the addition of complexes **1** and **2**, the positive band decreased in intensity with a concomitant red shift to 280 nm while negative band (245 nm) increased in intensity (Fig. S20), suggested that complexes **1** and **2** could unwind the DNA helix and lead to the loss of helicity. The complex **2** registered more decrease in the CD band intensity than **1** at the same concentration which implies that complex **2** is more effective in perturbing the secondary structure of DNA.

3.6. DNA cleavage studies

To assess the DNA cleavage ability of complexes **1** and **2**, supercoiled pBR322 DNA was incubated with varying concentration of complexes in 5 mM Tris – HCl/50 mM NaCl buffer at pH 7.2 for 1 h in the absence of any reducing agent. Upon successive addition of complexes **1** and **2**, supercoiled form (SC Form I) of DNA was gradually converted into slower – moving nicked circular form (NC Form II) (Lane 2 – 4 for **1** and 7-10 for **2**). When the concentration of complex **1-2** reached to 25 μM (Lane 6 for **1** and 11 for **2**), the Form I was completely converted into Form II without the formation of linear circular form (LC Form III), which migrates in between SC and NC form (Fig. 4) revealing single strand DNA cleavage [44].

The mechanistic cleavage activity of complexes **1** and **2** was analyzed in presence of activators *viz.* H_2O_2, ascorbate (ASC), 3-mercaptopropionic acid (MPA) and glutathione (GSH). The cleavage activity was significantly enhanced by these activators in the order H_2O_2 > GSH > MPA > ASC (Fig. S21). Furthermore, to elucidate the DNA cleavage pathway, reactions of complexes **1** and **2** were carried out in presence of ROS scavengers *viz.*, hydroxyl radical scavenger (DMSO and EtOH), singlet oxygen quencher (NaN_3) and super oxide scavenger (SOD) (Fig. S22). It was observed that DMSO and EtOH did not show any apparent inhibition of the DNA strand scission, ruling out the possibility of involvement of diffusible hydroxyl radicals

in the cleavage reaction. However, in presence of NaN_3, significant inhibition was observed which revealed that ROS species *viz*., singlet oxygen, $^1O_2$ was responsible for the DNA cleavage process *via*. oxidative pathway [45].

To further confirm the binding of the complexes **1** and **2** with the DNA helix, the cleavage reactions with minor groove binder, DAPI and major groove binder, methyl green (MG) were carried out (Fig. S21). There was no apparent inhibition of DNA damage with methyl green in presence of complexes **1** and **2**, while significant inhibition of DNA cleavage in presence of DAPI was observed implicating the binding of the complexes to DNA in the minor groove of DNA double helix. These results were also substantiated by molecular docking experiments.

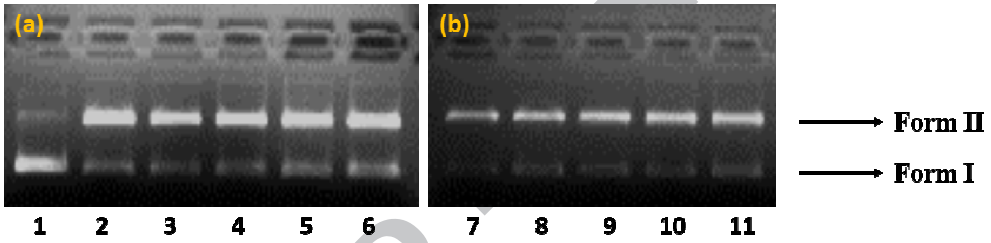

Fig. 4. Gel electrophoresis assay of complexes **1-2** with pBR322. (a) Cleavage of pBR322 plasmid DNA (300ng) by complex **1** in 50 mM Tris–HCl/NaCl buffer (pH, 7.3) after 40 min exposure time at different concentration; Lane 1: DNA control; Lane 2: 5 μM **1** + DNA; Lane 3: 10 μM **1** + DNA; Lane 4: 15 μM **1** + DNA; Lane 5: 20 μM **1** + DNA; Lane 6: 25 μM **1** + DNA. (b) Lane 7: 5 μM **2** + DNA; Lane 8: 10 μM **1** + DNA; Lane 9: 15 μM **1** + DNA; Lane 10: 20 μM **1** + DNA; Lane 11: 25 μM **1** + DNA.

3.8. Molecular docking

Since complexes **1** and **2** possess good DNA binding and significant cleaving activity, therefore molecular docking study was employed to investigate the preferable binding site of copper complexes to DNA helix. Moreover, molecular docking is a virtual computational method which provides the deeper insight of binding affinity and involvement of non-covalent interactions responsible for binding [46]. An energetically favorable docked pose obtained from the

molecular docking of complexes **1** and **2** with a DNA duplex of sequence d(CGCGAATTCGCG)$_2$ dodecamer (PDB ID: 1BNA) is shown in Fig. 10. Docking results revealed that DNA- complexes **1** and **2** were stabilized by forming non-covalent interactions mainly electrostatic and hydrophobic. The evaluation of docked model showed that complexes **1** and **2** snugly fitted in the minor groove (Fig 10 and S23). Additionally, the flexible alkyl arms of complexes **1** and **2** anchored the hydrophobic interior surface of DNA and derived various hydrophobic contacts. Relative binding energy of the docked structures of **1** and **2** was found to be -4.8 kcal/mol and -5.2 kcal/mol, respectively. Therefore, we can conclude that there is a good agreement between the experimental DNA binding results and molecular modelling calculations.

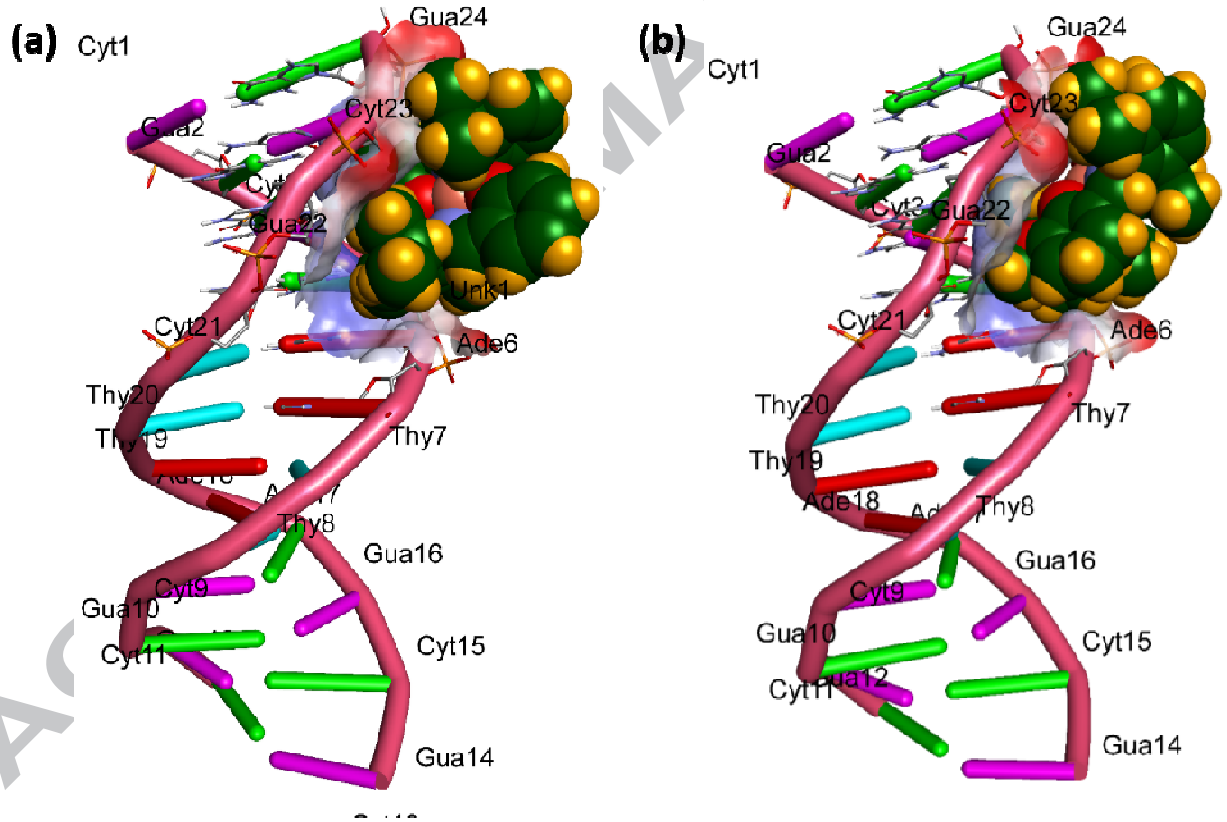

Fig. 5. Molecular docked model of (a) complex **1** and (b) complex **2** with the minor groove of DNA.

3.9. Bacterial anti-biofilm activity

The antibacterial activity of the complexes **1** and **2** was demonstrated by minimal inhibitory concentration (MIC) and was found to be 175 μg-ml^{-1} and 100 μg-ml^{-1} against gram negative bacteria *E. coli* 25922, respectively. MIC of the complexes was determined to select the sub-MICs to access the biofilm inhibitory effect of complexes against the test bacteria. Significant inhibition in biofilm formation was observed in test bacterial strain when tested in the presence of sub-MICs (12.5-50 μg-ml^{-1}) of complexes. At the highest tested concentration (50 μg-ml^{-1}), complexes **1** and **2** exhibited 47% and 65% reduction, respectively in biofilm formation (Table S5). The activity of copper complexes against biofilm was reasonably good at their sub-inhibitory concentrations, however, complex **2** showed comparatively better effects. Light microscopy and SEM analysis showed the formation of well-developed biofilm by untreated control, whereas the bacterial strain treated with the complexes **1** and **2** (50 μg-ml^{-1}) developed poor biofilm (Fig 6).

Earlier literature reports have shown that copper complexes exhibit antibiofilm activity against gram positive and gram negative bacteria [47]. Mechanistic insight of the antibiofilm activity of copper ions in the complexes suggested different mode of actions albeit, more prominently by DNA destruction, as extracellular and intracellular genetic materials play a pivotal role during the various stages of biofilm development and maturation [48]. It is implicated that DNA cleavage and membrane permeability play a critical role in determining the antibiofilm effect of different complexes [49]. Since bacterial plasmids are necessary for maintaining biofilm integrity and conferring the gene resistance among the biofilm community *via* horizontal gene transfer

[50], therefore the proven cleaving activity of complexes **1** and **2** could also be responsible for the inhibition of biofilms.

In complex **2**, enhanced antibiofilm effect could be attributed to the ligand, o-vanillin- a well-known membrane active metabolite, that affects the ion balance and normal respiratory functioning and ultimately leads to improved permeability with additional antibacterial effects specifically against *E. coli* [51]. Thus, the inhibition of biofilm forming ability of tested bacteria by these complexes is a coordinated affair, where each moiety in its own capacity and overall tailored metal-based drug entities induce the cumulative effect affecting the molecular machinery of bacterium. The present study highlighted the anti-infective potential of copper therapeutic agents based primarily on DNA damage and cleavage properties of copper chelated with bioactive organic ligand scaffold.

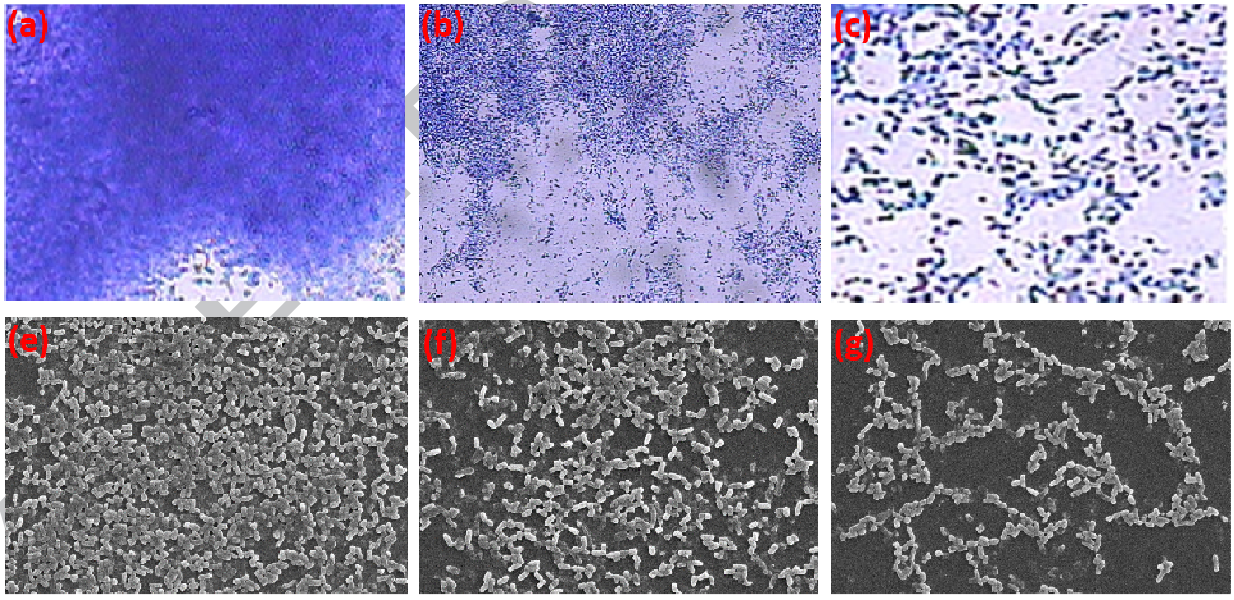

Fig. 6. Microscopic images of *E. coli* 25922 biofilm in the presence and absence of sub-MICs Complexes. (a) Light microscopic image of untreated control, (b) treated with 50 µg/ml of complex **1**, (c) treated with 50 µg/ml of complex **2**, (d) Scanning electron microscopic image of untreated control and (e) treated with 50 µg/ml of complex **1** and (f) treated with 50 µg/ml of complex **2**.

Conclusion

Copper-based therapeutic drug entities, $[Cu(dip)_2]$ (**1**) and $[Cu(dimp)_2]$ (**2**) have been synthesized and characterized thoroughly by single crystal X-ray diffraction analysis and other spectroscopic techniques. The crystal structure and Hirshfeld surface analysis revealed the molecular assembly of complexes **1** and **2** stabilized through H···H, C···H and H···H, O···H, C···H, O···C and rare C-H···Cu anagostic type of non-covalent forces, respectively. The biological relevance of various low energy out-of-plane vibrational mode of copper skeletal have been assigned to below 200 cm^{-1} range of wavenumber. *In vitro* DNA binding profile of complexes **1** and **2** revealed the electrostatic mode of binding with partial intercalation in minor groove region. Additionally, molecular docking studies have been performed to corroborate the trend of DNA binding site and affinity of the complexes **1** and **2** which is in good agreement with the experimental findings. The complexes **1** and **2** having the ability of DNA cleavage through an oxidative mechanism induced by reactive oxygen species (ROS). Additionally, antibiofilm activity of complexes **1** and **2** was evaluated against *E. coli* 25922. The complex **2** showed 65% reduction in biofilm formation of *E. coli* 25922 at 50 µg/ml while complex **1** exhibited 47%, which could be due to the extracellular DNA binding ability of the complexes. Thus, the results of anti-biofilm activity experiment validated that copper complexes is a potent drug entity and could be employed against bacterial biofilm infections.

Acknowledgements

The authors are grateful to SAIF Panjab University, Chandigarh, for providing ESI–MS and elemental analysis facility. We are also thankful to Department of Chemistry and USIF, Aligarh Muslim University for providing the FT-IR, UV-vis, EPR and SEM facility. The author (Mohammad Usman) sincerely acknowledges financial support from University Grants

Commission (UGC), New Delhi, for providing the fellowship and the Department of Chemistry, AMU through UGC assisted DRS–SAP, DST -FIST and DST PURSE Programme.

References

1. (a) L. H. Stoodley, J. William Costerton, Paul Stoodley, *Nature Reviews Microbiology*, 2 (2004) 95. (b) G. W. Amsden, *J Antimicrob Chemother*. 55 (2005) 10. (c) R. M. Donlan, *Emerg Infect Dis*. 2 (2001) 277. (d) M. R. Parsek, *Annu. Rev. Microbiol.* 57 (2003) 677. (e) P. Naves, G. del Prado, L. Huelves, V. Rodríguez-Cerrato, V. Ruiz, M.C. Ponte, F. Soriano, *Journal of Hospital Infection*. 76 (2010) 165.

2. N. Hoiby, T. Bjarnsholt, C. Moser, G. L. Bassi, T. Coenye, G. Donelli, L. Hall-Stoodley, V. Hola, C. Imbert, K. Kirketerp-Moller, D. Lebeaux, A. Oliver, A. J. Ullmann, C. Williams, *Clin Microbiol Infect.* 21 (2015) 1.

3. L. Viganor, A. C. M. Galdino, Ana Paula F. Nunes, Katia R. N. Santos, Marta H. Branquinha, Michael Devereux, Andrew Kellett, Malachy McCann, Andre L. S. Santos, *J Antimicrob Chemother*. 71 (2016) 128.

4. (a) A. Bolhuis, J. R. Aldrich-Wright, *Bioorg. Chem.* 55 2014 51. (b) S. K. Boda, S, Pandit, A. Garai, D. Pal, B. Basu, *RSC Adv*. 6 (2016) 39245.

5. (a) R. P. Lange, H. H. Locher, P. C. Wyss, R. L. Then, *Curr. Pharm. Des.* 13 (2007) 3140. (b) M. Zaki, F. Arjmand and S. Tabassum, *Inorganica Chimica Acta.* 444 (2016) 1.

6. (a) H. Mulcahy, L. Charron-Mazenod and Shawn Lewenza, *PLoS Pathogens*. 4 (2008)1. (b) A. Seper, V. H. I. Fengler, S. Roier, H. Wolinski, S. D. Kohlwein, A. L. Bishop, A. Camilli, J. Reidl, S. Schild, *Molecular Microbiology*. 82 (2011) 1015. (c) D. Frees, A. Chastanet, S. Qazi, K. Sorensen, P. Hill, T. Msadek, H. Ingmer, *Mol Microbiol*. 54 (2004) 1445. (d) R. V. Houdt, C. W. Michiels, *Research in Microbiology*. 156 (2005) 626.

7. (a) P. C. Bruijnincx, P. J. Sadler, *Curr. Opin. Chem. Biol.*, 12 (2008) 197. (b) T. W. Hambley, *Dalton Trans.* (2007) 4929.

8. A. C. Komor, J. K. Barton, *Chem. Commun*. 49 (2013) 3617.

9. (a) K. G. Daniel, R. H. Harbach, W. C. Guida, Q. P. Dou, *Front. Biosci.* 9 (2004) 2652. (b) Y. Fu, F.M. J. Chang, D. P. Giedroc, *Acc. Chem. Res*. 47 (2014) 3605.

10. (a) N. Vassallo, J. W. Herms, *J. Neurochem.* 86 (2003) 538. (b) M. L. Turski, D. J. Thiele, *J. Biol. Chem.* 284 (2009) 717.

11. N. Graf and S. J. Lippard, *Adv. Drug Deliv. Rev.* 64 (2012) 993.

12. (a) C. Santini, M. Pellei, V. Gandin, M. Porchia, F. Tisato, C. Marzano, *Chem. Rev*. 114 (2014) 815. (b) T. Storr, K. H. Thompson, C. Orvig, *Chem. Soc. Rev*. 35 (2006) 534.

13. (a) E. Halevas, O.Tsave, M.P. Yavropoulou, A. Hatzidimitriou, J.G.Yovos, V. Psycharis, C. Gabriel, A.Salifoglou, J. Inorg. Bio. 147 (2015) 99. (b) K. Lirdprapamongkol, J.Peterkramb, T. Suthiphongchai, R. Surarit, C. Srisomsap, G. Dannhardt, J. Svasti, *J. Agric. Food Chem*. 57 (2009) 3055. (c) J. Vanco, J. Marek, Z. Travnicek, E. Racanska, J. Muselik, O. Svajlenova, *J. Inorg. Biochem*. 102 (2008) 595. (d) C. Patra, A.K. Bhanja, C. Sen, D. Ojha, D. Chattopadhyay, A. Mahapatra, C. Sinha, Sensors Actuators B Chem., 228 (2016), 287. (e) A.K. Bhanja, C. Patra, S. Mondal, D. Ojha, D. Chattopadhyay, C. Sinha, RSC Adv., 5 (2015), 48997.

14. (a) H. J. Schneider, Angew. Chem. Int. Ed. 48 (2009) 3924. (b) L. M. Salonen, M. Ellermann, F. Diederich, *Angew. Chem*. Int. Ed. 50 (2011) 4808.

15. (a) D. Paolantoni, J. Rubio-Magnieto, S. Cantel, J. Martinez, P. Dumy, M. Surin, S. Ulrich, *Chem. Commun*. 50 (2014) 14257. (b) C. Estarellas, A. Frontera, D. Quiaeonero, P. M. Deya, Angew. Chem. Int. Ed. 50 (2011) 415. (c) A. Frontera, P. Gamez, M. Mascal, T. J. Mooibroek, J. Reedijk, *Angew. Chem*. Int. Ed. 50 (2011) 9564.

16. Software Users Guide, v. 6.0, Bruker Analytical X-ray Systems, Madison, WI, 1999; G. M. Sheldrick, SADABS: Area-Detector Absorption Correction, v. 2.03, University of Gottingen, Gottingen, Germany, 1999; SADABS, v. 2008.

17. G. M. Sheldrick, SHELX–97, *Program for Crystal Structure refinement, University of Gottingen*, Germany, 1997.

18. (a) F. Neese, *WIREs Comput. Mol. Sci.* 2 (2012) 73. (b) F. Neese, "Orca. *An ab Initio, Density Functional and Semiempirical Program Package version",* (2009).

19. C. Lee, W. Yang. R. G. Parr, *Phys. Rev. B*. 37 (1988) 785.

20. (a) F. Weigend and R. Ahlrichs, *Phys. Chem. Chem. Phys.* 7 (2005) 3297. (b) A. Schaefer, C. Huber and R. Ahlrichs, *J. Chem. Phys*. 100 (1994) 5829. (c) A. Schaefer, H. Horn, R. Ahlrichs, *J. Chem. Phys*. 97 (1992) 2571.

21. (a) S. Grimme, J. Antony, S. Ehrlich and H. Krieg, *J. Chem. Phys.* 132 (2010) 154104 . (b) C. Steffen, K. Thomas, U. Huniar, A. Hellweg, O. Rubner, A. Schroer, *J. Comput. Chem.* 31 (2010) 2967.

22. M. A. Spackman, D. Jayatilaka, *CrystEngComm.* 11 (2009) 19.

23. (a) O. Trott, A. J. Olson, J. Comput. Chem. 31 (2010) 455. (b) M. F. Sanner, *J. Mol. Graphics Mod*. 17 (1999) 57.

24. (a) Accelrys Software Inc., Discovery Studio Modeling Environment, Release 4.0, San Diego: Accelrys Software Inc., 2013. (b) The PyMOL Molecular Graphics System, Version 1.5.0.4 Schrödinger, LLC.

25. (a) J. Murmurs, *J. Mol. Biol*. 3 (1961) 208. (b) M. E. Reicmann, S. A. Rice, C. A. Thomas, P. Doty, *J. Am. Chem. Soc.* 76 (1954) 3047.

26. F. Arjmand, M. Muddassir, R. H. Khan, *Eur. J. Med. Chem*. 45 (2010) 3549.

27. G. A. O. Toole, R. Kolter, *Mol Microbiol*. 30 (1998) 295.

28. I.A.S.V. Packiavathy, P. Agilandeswari, K.S. Musthafa, S.K. Pandian, A.V. Ravi, *Food Research International.* 45 (2012) 85.

29. (a) K. Sundaravel, E. Suresh, M. Palaniandavar, *Inorg. Chim. Acta*. 362 (2009) 199. (b) A. Upadhyay, S. Vaidya, V. S. Venkatasai, P. Jayapal, A. K. Srivastava, M. Shanmugam M. Shanmugam, *Polyhedron*. 66 (2013) 87.

30. M. Enamullah, A. K. M. Royhan Uddin, G. Pescitelli, R. Berardozzi, G. Makhloufi, V. Vasylyeva, A.C. Chamayou, C. Janiak, *Dalton Trans*. 43 (2014) 3313.

31. C. Fliedel, V. Rosa, C. I. M. Santos, P. J. Gonzalez, R. M. Almeida, C. S. B. Gomes, P. T. Gomes, M. A. N. D. A. Lemos, G. Aullon, R. Welter, T. Aviles, *Dalton Trans*. 43 (2014) 13041.

32. R. Kannappan, S. Tanase, I. Mutikainen, U. Turpeinen, J. Reedijk, *Inorg. Chim. Acta*. 358 (2005) 383.

33. D. N. Kumar, B. K. Singh, B. S. Garg, P. K. Singh, *Spectrochim. Acta*, *Part A*, 59 (2003) 1487.

34. S. Ramakrishnan, D. Shakthipriya, E. Suresh, V. S. Periasamy, M. A. Akbarsha, M. Palaniandavar, *Inorg. Chem*. 50 (2011) 6458.

35. (a) C. Ravikumar, I. H. Joe, V. S. Jayakumar, *Chem. Phys. Lett*. 460 (2008) 552. (b) W. M. Al-Asbahy, M. Usman, F. Arjmand, M. Shamsi, S. Tabassum, *Inorg. Chim. Acta*. 445 (2016) 167.

36. (a) D. F. V. Lewis, C. Ioannides, D. V. Parke, *Xenobiotica*, 24 (1994) 401. (b) P. Thanikaivelan, V. Subramanian, J. R. Rao, B. U. Nair, *Chem. Phys. Lett*. 323 (2000) 59.

37. (a) M. Brookhart, M.L.H. Green, G. Parkin, Proc. Natl. Acad. Sci. USA 104 (2007) 6909. (b) V. Singh, R. Chauhan, A. N. Gupta, V. Kumar, M. G. B. Drew, L. Bahadur N. Singh, *Dalton Trans*. 43 (2014) 4752.

38. (a) M. Ganeshpandian, R. Loganathan, E. Suresh, A. Riyasdeen, M.A. Akbarshad, M. Palaniandavar, *Dalton Trans*. 43 (2014) 1203 (b) R. Manikandan, N. Chitrapriya, Y. J. Jang, P. Viswanathamurthi, *RSC Adv*. (2013) 11647.

39. A. Wolfe, G. H. Shimer, T. Meehan, *Biochemistry*. 26 (1987) 6392.

40. C. Liu, J. Zhou, H. Xu, *J. Inorg. Biochem.* 71 (1998) 2.

41. P. Kumar, S. Gorai, M. K. Santra, B. Mondal, D. Manna, *Dalton Trans*. 41 (2012) 7573.

42. J. R. Lakowicz, G. Weber, *Biochemistry*. 12 (1973) 4161.

43. J. Kypr, I. Kejnovská, D. Renčiuk, M. Vorlíčková, *Nucleic Acids Res.* 37 (2009) 1713.

44. S. Tabassum, A. Asim, F. Arjmand, M. Afzal, V. Bagchi, *Eur. J. Med. Chem.* 58 (2012) 308.

45. M. S. Melvin, M. W. Calcutt, R. E. Noftle, R. A. Manderville, *Chem. Res. Toxicol.* 15 (2002) 742.

46. B. K. Shoichet, S. L. McGovern, B. Wei, J. J. Irwin, *Curr. Opin. Chem. Biol.* 6 (2002) 439.

47. (a) S. L. Warnes, V. Caves, C. W. Keevil, *Environmental Microbiology*. 14 (2012) 1730. (b) J. A. Lemire, J. J. Harrison, R. J. Turner, *Nat. Rev. Microbiol*. 11 (2013) 371.

48. M. L. Beeton, J. R. A. Wright, A. Bolhuis, *J Inorg Biochem*. 140 (2014) 167.

49. (a) J. S. Madsen, M. Burmolle, L. H. Hansen, S. J. Sorensen, *FEMS Immunol Med Microbiol*. 65 (2012) 183. (b) C. B. Whitchurch, T. Tolker-Nielsen, P. C. Ragas, J. S. Mattick, *Science*. 295 (2002) 1487.

50. J. M. Ghigo, *Nature*. 412 (2011) 442.

51. (a) D.J. Fitzgerald, M. Stratford, M.J. Gasson, J. Ueckert, A. Bos, A. Narbad, *J. Appl. Microbiol*. 97 (2004) 104. (b) A. O. Gill, R. A. Holley, *Int. J. Food Microbiol*. 108 (2006) 1.

DNA minor groove targeted copper(II) complexes explored as an antibiofilm active agents against *E. Coli* 25922.

Graphical abstract

Antibiofilm activity and docking model of Copper complex

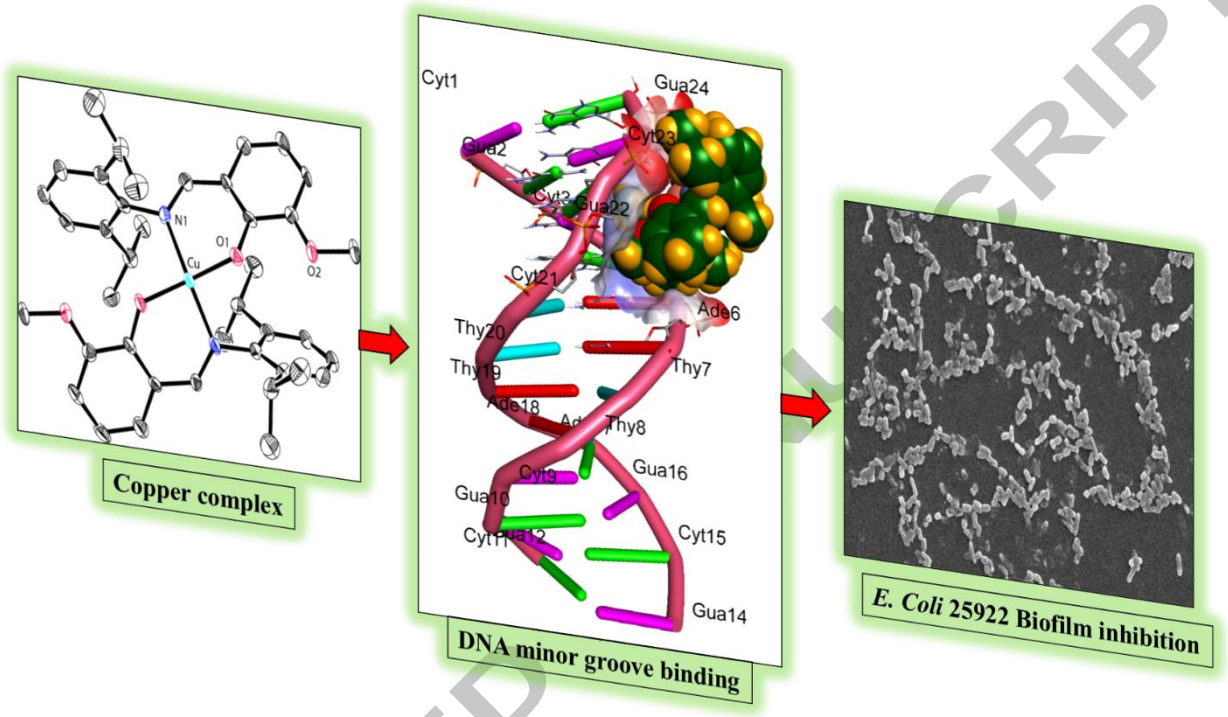

- Two mononuclear Copper(II) complexes, $[Cu(dip)_2]$ (**1**) and $[Cu(dimp)_2]$ (**2**) have been synthesized and characterized thoroughly by various spectroscopic methods (EPR, FTIR and UV-vis) techniques and single crystal X-ray diffraction analysis.
- Dispersion corrected B3LYP/DFT calculations have been carried out to elucidate the tentative assignments of N-Cu-N/O-Cu-O/O-Cu-N and other significant vibrational modes.
- Hirshfeld surface analyses to explore H-bonding, C-H/π and Cu…H-C interactions.
- Copper complexes damaged pBR322 plasmid DNA by oxidative pathway via ROS species *viz*., $O_2^{\bullet-}$, $^1O_2$ etc.
- Antibiofilm activity was evaluated against *E. Coli* 25922.